Traffic

Published by John Wiley & Sons Ltd
doi:10.1111/tra.12334

Vps33B is required for delivery of endocytosed cargo to lysosomes

Romain Galmes[1,2], Corlinda ten Brink[1], Viola Oorschot[1,3], Tineke Veenendaal[1], Caspar Jonker[1], Peter van der Sluijs[1] and Judith Klumperman[1]*

[1]Department of Cell Biology and Institute of Biomembranes, Center for Molecular Medicine, University Medical Center Utrecht, Heidelberglaan 100, 3584CX Utrecht, The Netherlands
[2]Present address: Institut Jacques Monod, CNRS, UMR7592, Université Paris Diderot, Sorbonne Paris Cité, F-75013 Paris, France
[3]Present address: Monash Micro Imaging, 15 Innovation Walk, Strip 1 Monash Biotechnology, Monash University, Clayton, VIC 3800, Australia
*Corresponding author: Judith Klumperman, j.klumperman@umcutrecht.nl

Abstract

Lysosomes are the main degradative compartments of eukaryotic cells. The CORVET and HOPS tethering complexes are well known for their role in membrane fusion in the yeast endocytic pathway. Yeast Vps33p is part of both complexes, and has two mammalian homologues: Vps33A and Vps33B. Vps33B is required for recycling of apical proteins in polarized cells and a causative gene for ARC syndrome. Here, we investigate whether Vps33B is also required in the degradative pathway. By fluorescence and electron microscopy we show that Vps33B depletion in HeLa cells leads to significantly increased numbers of late endosomes that together with lysosomes accumulate in the perinuclear region. Degradation of endocytosed cargo is impaired in these cells. By electron microscopy we show that endocytosed BSA-gold reaches late endosomes, but is decreased in lysosomes. The increase in late endosome numbers and the lack of internalized cargo in lysosomes are indicative for a defect in late endosomal–lysosomal fusion events, which explains the observed decrease in cargo degradation. A corresponding phenotype was found after Vps33A knock down, which in addition also resulted in decreased lysosome numbers. We conclude that Vps33B, in addition to its role in endosomal recycling, is required for late endosomal–lysosomal fusion events.

Keywords HOPS complex, late endosomes, lysosomes, SM proteins, Vps33A, Vps33B

Received 12 March 2015, revised and accepted for publication 16 September 2015, uncorrected manuscript published online 25 September 2015, published online 21 October 2015

Lysosomes are the main degradative compartments of eukaryotic cells, responsible for degradation of endocytosed material as well as intracellular components. Degradation of endocytosed cargo requires transport from the plasma membrane to lysosomes via a sequence of steps: transport to early endosomes (EEs), EE homotypic fusion, maturation of EEs into late endosomes (LEs), LE homotypic fusion and LE-lysosome fusion. A crucial step of EE maturation is the substitution of the EE Rab5 GTPase by the LE Rab7 GTPase, which provides LEs with the competence to fuse with lysosomes (1–3). In addition, maturing endosomes acquire lysosomal enzymes, an acidic environment, and the protein machinery required for lysosomal fusion events (4–6).

Membrane fusion events are tightly regulated by a set of machinery proteins including Rab GTPase proteins, soluble *N*-ethylmaleimide-sensitive factor attachment protein receptors (SNARE) proteins and single long coiled-coiled or multi-subunit tethering factors (7,8). After activation, Rab GTPases recruit tethering complexes that bring membranes of two compartments into close proximity, a crucial step for fusion (9). Then, proteins of the Sec1/Munc18 (SM) family promote interactions between specific SNARE

combinations, leading to the formation of a trans-SNARE complex and subsequently fusion of the two compartments (10,11). The mechanism by which SM proteins promote this interaction is not well-understood (12).

In yeast the endosomal Class C core vacuole/endosome transport (CORVET) and the vacuolar homotypic fusion and vacuole protein sorting (HOPS) complexes function as tethers in the endo-lysosomal system (13–19). The CORVET and HOPS complexes share a core of four class C vacuolar protein sorting (Vps) proteins: Vps11p, Vps16p, Vps18p and Vps33p. In addition, the CORVET complex contains Vps3p and Vps8p, while the HOPS complex contains Vps39p and Vps41p (20–22). Vps8p and Vps41p interact with activated yeast homologues of Rab5 and Rab7, respectively, which contributes to the localization of the CORVET complex to endosomes and the HOPS complex to the vacuole, the yeast lysosome (13,17,23,24). In addition, Vps41p binds acidic phospholipids, enhancing membrane association of the HOPS complex to the vacuole (25). The core subunit Vps33p is a SM protein that binds the SNARE proteins Pep12p on endosomes and Vam3p on the vacuole (26–28). Recent studies have shown that within both yeast CORVET and HOPS complexes, Vps33p interacts with Vps16p (21,29,30). Together, CORVET and HOPS mediate membrane fusion events within the yeast endo-lysosomal system.

All CORVET/HOPS complex subunits have mammalian homologues, showing that these complexes are highly conserved. However, the existence of mammalian specific homologues of Vps33p (Vps33A and Vps33B) and Vps16p (Vps16/Vps16A and VIPAS-39/Vps16B), suggests additional or alternative functions of these complexes or subunits in membrane traffic (31–34). Human Vps33A and B share 32% identity and 51% homology. Vps33A binds specifically to Vps16A while Vps33B interacts only with VIPAS-39 (Vps33B-interacting protein, apical-basolateral polarity regulator, spe-39 homolog, also known as Vps16B) (35–38).

Several studies indicate that Vps33A and B have overlapping yet different functions in membrane trafficking. In *Drosophila melanogaster*, Pulipparacharuvil et al. (35) were the first to show that dVps33A (Car) and dVps33B interact exclusively with dVps16A and dVps16B (fob), respectively. The specificity of these interactions was confirmed in mammalian cells (v.d. Kant et al, in submission, 38, 39). Both dVps16A and dVps16B (fob) interact with dVps18, indicating that there are two Vps C-like protein complexes that co-exist in the cell (35). Furthermore, *Caenorhabditis elegans* contains two Vps33 homologues with Vps33.1 being part of the HOPS complex and Vps33.2 of the CORVET complex (40). It is still unclear whether VPS33.1 and VPS33.2 are direct orthologous of Vps33A and Vps33B or evolutionarily different.

In *Drosophila* as well as mice both Vps33A (Car) and Vps16A are required for the delivery of endocytosed cargo to lysosomes (35,41–44) as mutations or loss of either protein induces accumulation of endocytosed ligands in LAMP-1- and Rab7-positive LEs. In mammalian cells, Vps33A mutations impair biogenesis of lysosome-related organelles (LROs), like δ-granules in platelets and melanosomes in pigment cells, and Vps33A was recently identified as a crucial factor in autophagosome-lysosome fusion by interacting with syntaxin 17 (45). Studies from our own lab and others have shown that Vps33A and Vps16A, but not Vps33B and VIPAS-39 interact, with other HOPS subunits (v.d. Kant et al., in submission, 39). These data suggest a role for Vps33A but not Vps33B in LE-lysosome fusion as part of a mammalian HOPS complex. Recent studies showed that Vps33A and Vps16 are also part of the mammalian CORVET complex, containing Vps8 and TGFBRAP1/Vps3 as specific subunits (v.d. Kant et al., in submission, 46). Thus, Vps33A and Vps16A are part of both the CORVET and HOPS complexes of mammalian cells.

Mutations of either Vps33B or VIPAS-39 cause Arthrogryposis, Renal dysfunction and Cholestasis (ARC) syndrome, a rare recessive autosomal disease that predominantly affects platelets and polarized cells (36,47,48). When Vps33B is expressed together with VIPAS-39 the complex localizes to Rab11A-positive recycling endosomes, which are involved in recycling of apical membrane proteins and tight/adherent junction proteins in polarized cells (49–51). Accordingly, VIPAS-39- or Vps33B-deficient polarized mouse cells display defects in apical protein targeting and do not have functional tight junctions. However, similar to Vps33A function, Vps33B and VIPAS-39 are also required for LRO formation: Vps33B-knock down (KD)

megakaryocytes or platelets from ARC patients with mutations in VIPAS-39 lack α-granules, a second type of LRO of platelets (52,53). In addition, *Drosophila* dVps33B and dVps16B have been implicated in phagosome-lysosome fusion and phagosome acidification (54,55). Finally, depletion of VIPAS-39 in mammalian cells induces increased number of LAMP-1-positive compartments indicating a role of VIPAS-39 at late endosomal/lysosomal levels (36).

Together these data indicate that mammalian Vps33B together with VIPAS-39 forms a subcomplex involved in endosomal recycling, LRO formation and phagolysosome fusion. However, it is not yet known if VPS33B in mammals is involved in the endo-lysosomal pathway. Here we address the question if Vps33B, like Vps33A and yeast Vps33p, is involved in lysosome biogenesis. We show that knockdown of Vps33B impairs LE-lysosome fusion and cargo degradation and conclude that in addition to its known role in endosomal recycling Vps33B also acts in endo-lysosomal fusion events.

Results

Vps33B knockdown induces accumulation of LAMP1-positive compartments in the perinuclear area

To study the role of mammalian Vps33B in the endo-lysosomal pathway, we depleted HeLa cells of Vps33B for 3 days using siRNA. This resulted in an average of 75–90% decrease in both Vps33B mRNA (not shown) and protein levels (Figure 1A). Importantly, the mRNA levels of Vps33A and the HOPS specific subunit Vps41 were not affected by Vps33B knockdown (KD) and inversely (not shown). Cells were incubated with the fluorescent endocytic marker dextran-alexa568 for 2 h to visualize the endocytic pathway and transfected with LAMP-1-mGFP to monitor the transport and lysosomal targeting of newly synthesized lysosomal membrane proteins.

In control cells (scrambled siRNA-treated), LAMP-1-mGFP appeared as fluorescent spots or rings with dextran in their lumen (Figure 1C, upper panels). Vps33B depletion resulted in an accumulation of LAMP-1-mGFP-positive compartments in the perinuclear area (Figure 1C, lower panels), whereas dextran retained an overall dispersed distribution. Dextran-positive endosomes were seen in close opposition to LAMP-1-mGFP-positive/dextran-negative compartments (Figure 1C, lower panel). Quantification of the data revealed that 77% of transfected cells displayed an accumulation of LAMP-1-mGFP-positive compartments in the perinuclear area after Vps33B depletion (Figure 1B). Labeling of endogenous LAMP-1 in Vps33B KD cells showed a similar, although less prominent increase in number of LAMP-1-positive compartments in the perinuclear area (Figure 2), which confirms this phenotype. In contrast to Vps33B, Vps33A KD did not significantly change the localization pattern of LAMP-1 (45, Figure 1D). Unfortunately, we found that over-expression of proteins in Vps33A KD cells, like LAMP-1-mGFP, was lethal. This prevented us to perform experiments requiring protein over-expression in Vps33A KD cells.

We conclude from these data that Vps33B depletion leads to an accumulation of LAMP-1 and LAMP-1-mGFP-positive compartments, which are only partially reached by internalized dextran within a period of 2 h.

Vps33B depletion induces accumulation of Rab7-positive compartments

To characterize the population of endosomal compartments accumulating upon Vps33B KD, we made use of the Rab5 to Rab7 GTPase switch that marks the conversion of EEs to LEs (1,56). Control and Vps33B KD cells were transfected with Rab5-eGFP or Rab7-eGFP (Figure 2). Cells were then fixed for immunofluorescence and labeled for endogenous LAMP-1.

In control cells, consistent with numerous previous studies, Rab5-eGFP was found more peripheral and dispersed than LAMP-1, with only limited colocalization between the two labels (Figure 2A). Rab7-eGFP partially overlapped with LAMP-1, especially in the perinuclear region of the cells (Figure 2B). Vps33B depletion induced the characteristic accumulation of LAMP-1 positive compartments in the perinuclear area, but only a few of these compartments were positive for Rab5-eGFP (Figure 2A,C). By contrast, a large portion of the accumulated LAMP-1 compartments were positive for Rab7-eGFP (Figure 2B,C). Together these data show that Vps33B depletion leads to an accumulation

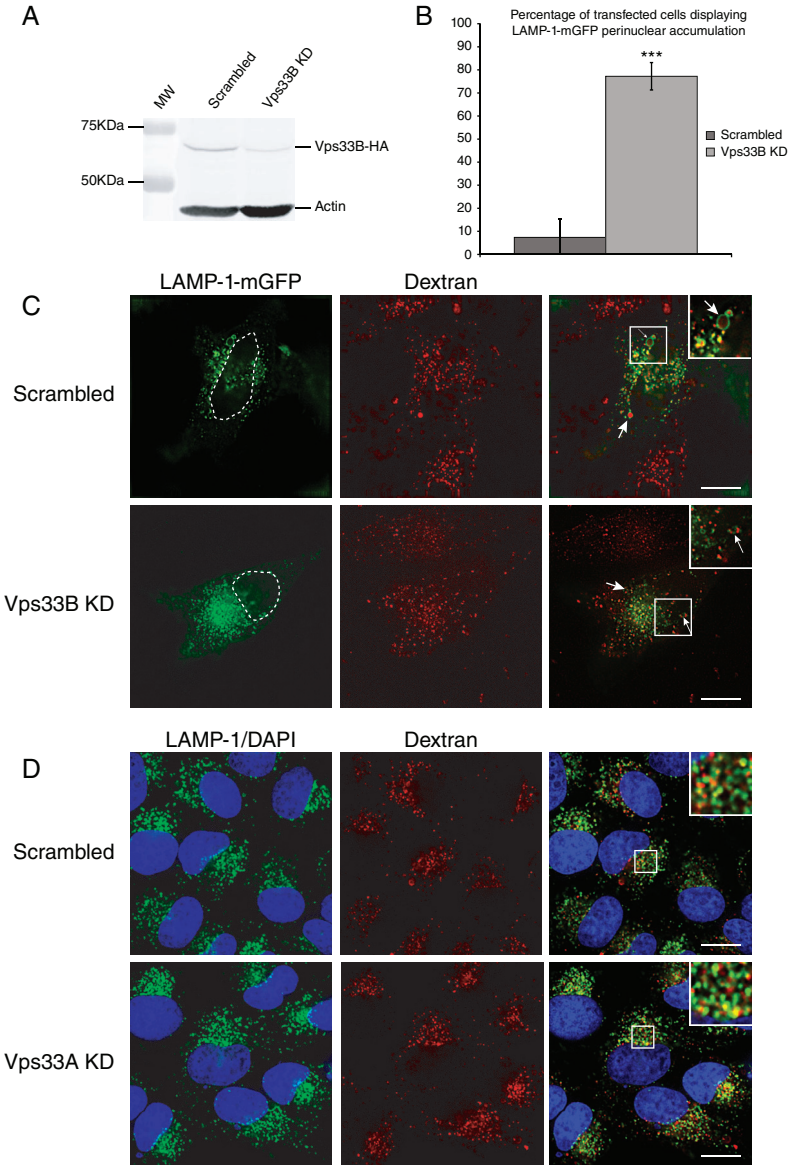

Figure 1: Vps33B depletion leads to the perinuclear accumulation of LAMP-1-mGFP compartments. A) HeLa cells were treated for 3 days with scrambled of Vps33B siRNA. KD efficiency was determined by western blot using anti-HA antibody on HeLa cells transiently transfected with Vps33B-HA. This showed an average decrease of 75% in Vps33B-HA protein expression after quantification by ImageJ. B) Quantification of the percentage of cells displaying an accumulation of LAMP-1-mGFP compartments in the perinuclear area in scrambled ($n = 75$ cells) or in Vps33B KD cells ($n = 99$ cells). Error bars represent the standard deviation, p-values were analyzed using a 2-tailed t-test with equal variance and related to the scrambled sample. ***$p < 0.001$. C) Fluorescent images of LAMP-1-mGFP and endocytosed dextran for 2 h (red panels) in scrambled or Vps33B siRNA-treated HeLa cells. In Vps33B KD cells, LAMP-1-mGFP-positive compartments accumulate in the perinuclear area (nuclei indicated by dotted line). Arrows in the merged panels indicate fluorescent rings representing LEs with or without dextran. Scale bars, 15 μm. D) Fluorescent images of scrambled or Vps33A-depleted HeLa cells incubated for 2 h with dextran-alexa568 and immunostained with anti-LAMP-1 antibody. Nuclei were stained with DAPI. Scale bar, 15 μm.

of especially LEs and lysosomes, which are able to recruit Rab7. Furthermore, the Rab7 recruitment indicates that Vp33B depletion does not notably affect the Rab5 to Rab7 switch.

Vps33B KD results in increased numbers of LEs

To further analyze the compartments accumulating upon Vps33B depletion, we performed immuno-electron microscopy. Scrambled or Vps33B-depleted HeLa cells were transfected with LAMP-1-mGFP overnight and processed to ultrathin cryosections. In HeLa cells, LAMP-1-positive lysosomes can be distinguished by EM from LAMP-1 positive LEs by morphological criteria. Lysosomes are distinguished by the presence of multi-lamellar membrane sheets and amorphous (degraded) electron dense material, while endosomes are characterized by the presence of at least six intra-luminal vesicles (57,58). Using these criteria we found that the population of LAMP-1-mGFP-positive compartments accumulating upon Vps33B depletion was composed of both LEs and lysosomes (Figure 3) of a relatively small size. The LAMP-1-mGFP-positive endosomes were often found in a cluster, with their opposing membranes in close proximity. This phenotype is also observed after Vps39 depletion and, to a lesser extent, Vps41 depletion (58), and suggests a defect in homotypic late endosome fusion.

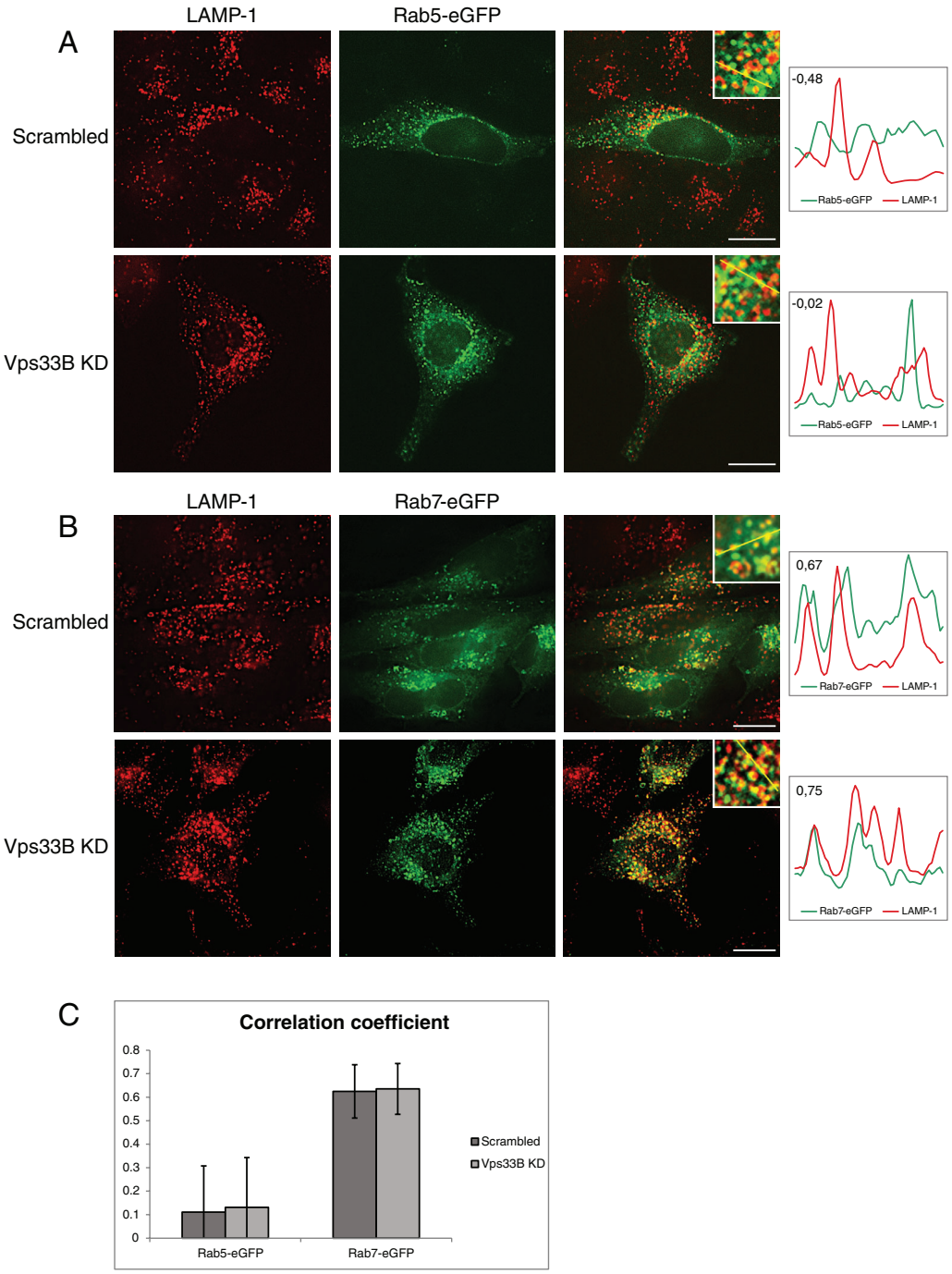

Figure 2: LAMP-1 positive compartments accumulating upon Vps33B KD are Rab7-positive and Rab5-negative. Scrambled or Vps33B KD HeLa cells, transfected with Rab5-eGFP (A) or Rab7-eGFP (B) for 8 h and labeled for endogenous LAMP-1 (red panels). Right panels show line profiles and the respective colocalization correlation coefficients of the line drawn in the higher magnification box. C) Quantification shows that accumulated LAMP-1 positive compartments in Vps33B KD cells colocalize with Rab7-, but not Rab5 ($n = 20$). Scale bars, 15 μm.

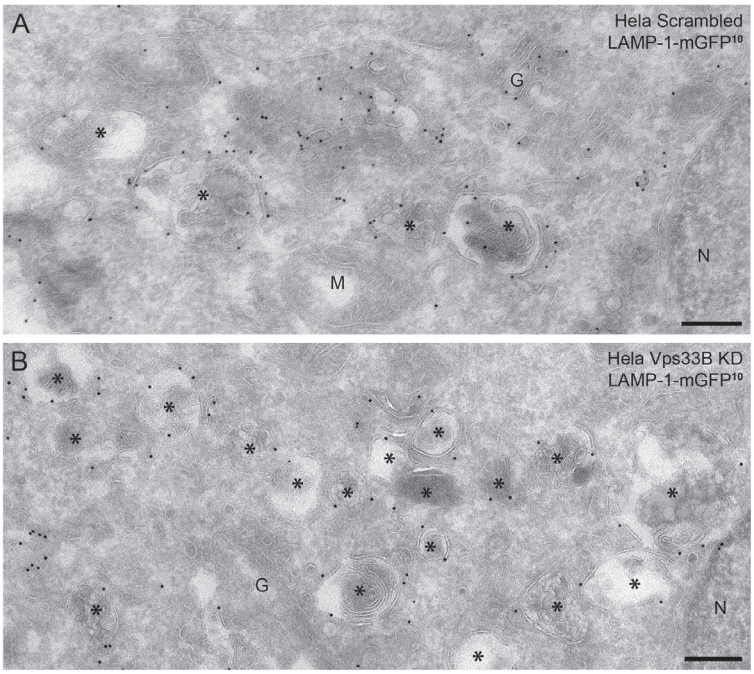

Figure 3: Vps33B KD leads to the clustering of LAMP-1-mGFP-positive endosomes and lysosomes. Electron micrographs of ultrathin cryosections of LAMP-1-mGFP transfected HeLa cell treated with scrambled (A) or Vps33B siRNAs for 3 days (B). Vps33B depleted cells show an accumulation and clustering of relatively small-sized LAMP-1-mGFP-positive LEs and lysosomes. Scale bars: 200 nm. *: late endosome/lysosome, N: nucleus.

To quantitatively assess the occurrence of LEs and lysosomes upon Vps33B KD, we labeled sections for endogenous LAMP-1 and counted the number of LAMP-1-positive endo-lysosomal compartments by randomly selecting cell sections containing a nuclear profile (i.e. to avoid samples of cellular tips, which often lack lysosomes). Our quantitation revealed a clear phenotype: upon Vps33B KD, the average number of LAMP-1-positive LEs was significantly increased (Figure 4A), whereas no change in lysosome numbers was seen.

For comparison, we performed a similar experiment in Vps33A KD cells (Figure 4B). These data showed that Vps33A KD also resulted in increased numbers of LAMP-1-positive endosomes. However, in contrast to Vps33B depletion, Vps33A KD also resulted in a significant decrease in lysosome numbers. Collectively these data discriminate the Vps33B KD phenotype from Vps33A, Vps39 and Vps41 KDs (58), by that Vps33B KD is the only condition that does not affect lysosome numbers. To study lysosome numbers and morphology in Vps33B KD cells by an alternative EM approach, we prepared flat-embedded Epon sections. The flat embedding procedure allows processing of the cells perpendicular to the growing plane, whereas the osmium fixation yields a differential contrast than cryosections (Figure 4C). Using this procedure, the presence of lysosomes upon Vps33B depletion was confirmed. However, in Vps33B KD cells, lysosomes had a less electron dense content and were smaller than in control cells, the latter confirming the observation by immunoEM (Figure 3).

Together, these data show that Vps33B KD induces increased numbers of LEs, which together with lysosomes accumulate in the perinuclear area. Lysosomes show an altered morphology but remain similar in number in Vps33B KD cells. The clusters of endosomes and lysosomes can still be reached by newly synthesized LAMP-1-mGFP, but – as shown in Figure 1C – less efficiently by endocytosed dextran after 2 h uptake.

Vps33B depletion leads to decreased degradation of endocytosed cargo

We next addressed whether depletion of Vps33B affects degradation of endocytosed cargo. Control or Vps33B KD cells were incubated for 4 h with dextran-alexa488 and DQ-BSA (Figure 5A). Like dextran-alexa488, DQ-BSA is taken up by fluid phase endocytosis, but unlike dextran-alexa488, DQ-BSA only becomes fluorescent after BSA degradation. The fluorescence intensity correlates with the number of free DQ molecules, which allows a quantitative assessment of degradation of endocytosed DQ-BSA. We used for this experiment an uptake time

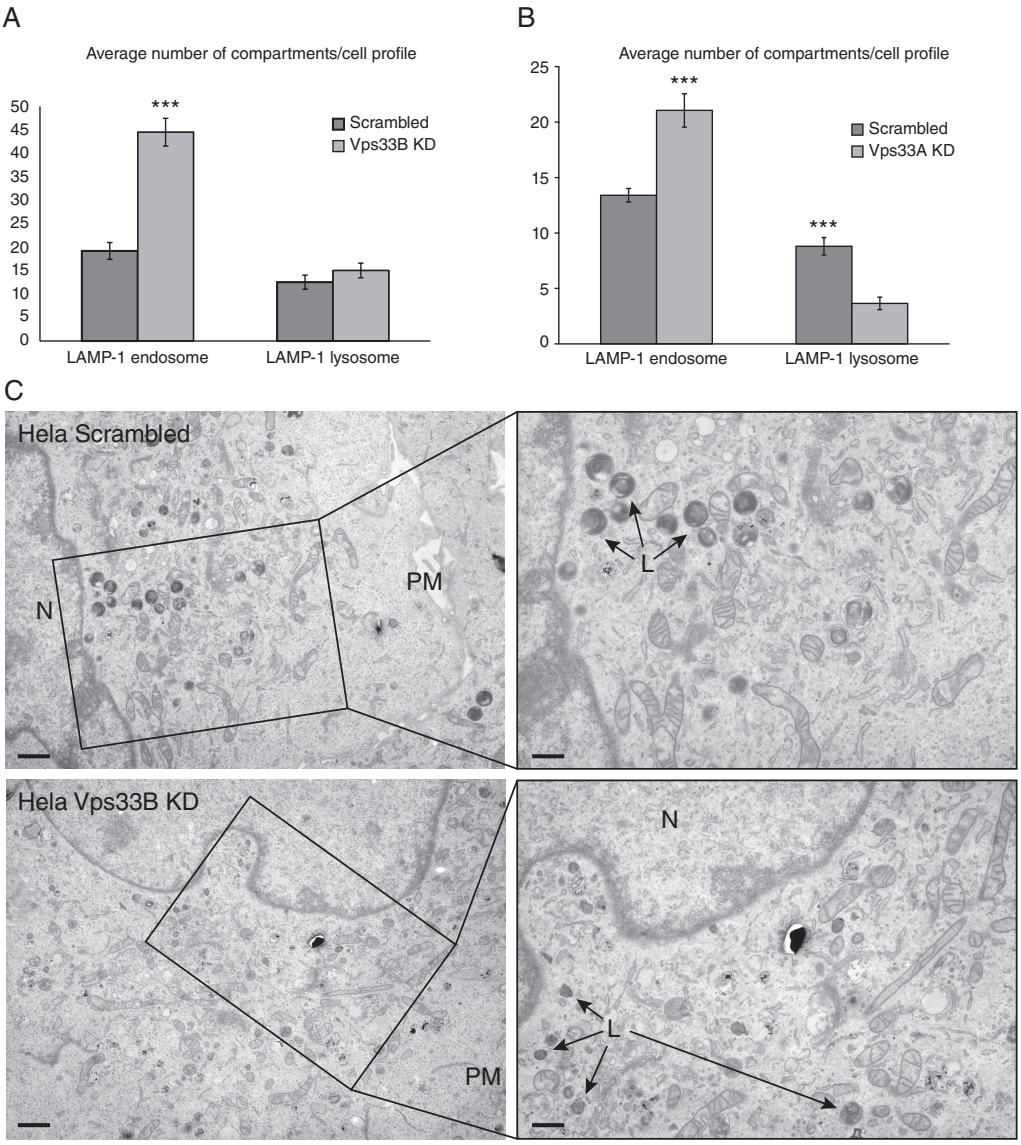

Figure 4: Vps33B KD leads to an increase in late endosome numbers. A) Quantification of the number of endosomes and lysosomes in HeLa cells scrambled siRNA-treated, Vps33B KD (A) or Vps33A KD (B). All endo-lysosomal compartments encountered in 20 random sampled cell profiles from two grids were characterized on bases of morphology and labeling for endogenous LAMP-1. This shows an increase of 2.3× [from 19.2 ± 1.79 to 44.5 ± 2.96 (SEM)] and 1.6× [from 13.4 ± 0.61 to 21.05 ± 1.5 (SEM)] of LAMP-1-positive endosomes per cell profile upon Vps33B KD and Vps33A KD, respectively. Interestingly, while lysosome numbers are not changed upon Vps33B KD, Vps33A KD induced a 2.4× decrease in LAMP-1-positive lysosomes (8.8 ± 0.68 in control cells versus 3.65 ± 0.56 (SEM) in Vps33A KD cells). Error bars represent the standard error of the mean, p-values were analyzed using a 2-tailed *t*-test with equal variance and related to the scrambled sample. ***$p < 0.001$. C) Electron micrographs of the perinuclear region of flat embedded scrambled siRNA-treated (upper panels) and Vps33B KD HeLa cells (lower panels) incubated for 2 h with BSA-Au[5]. In the absence of Vps33B, cells display smaller-sized lysosomes with a less electron dense content (arrows). N: nucleus, L: lysosome, PM: plasma membrane. Scale bars in left panels, 1 μm; scale bars in right panels, 500 nm.

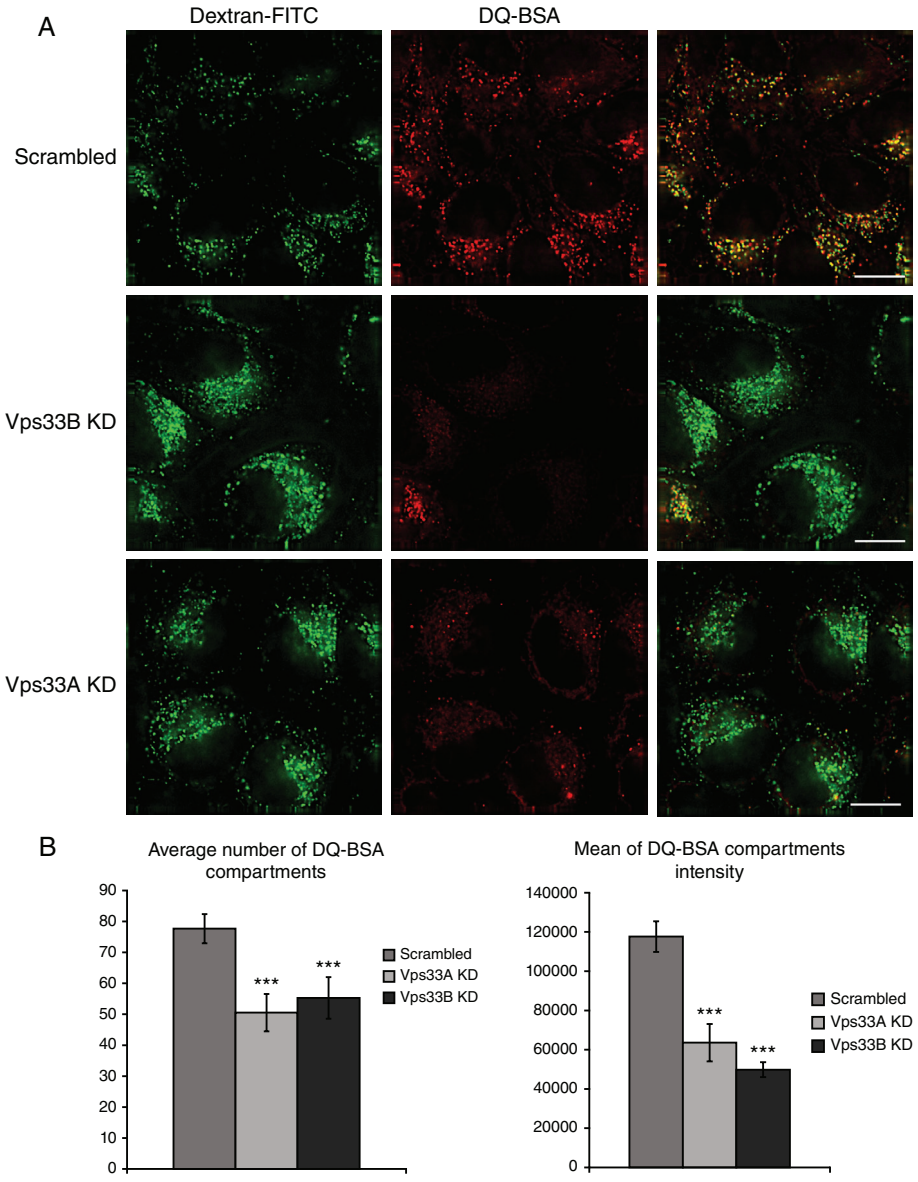

Figure 5: Vps33B KD decreases degradation of endocytosed cargo. A) Snapshot of live HeLa cells treated with scrambled, Vps33B or Vps33A siRNAs and incubated with DQ-BSA and FITC-conjugated dextran for 4 h. Only cleaved DQ-BSA molecules fluoresce, marking degradative endolysosomal compartments. Scale bars, 15 μm. B) Quantification per cell profile ($n = 36$ cells) shows a decrease in average number of fluorescent DQ-BSA compartments, from 77.67 ± 4.73 (SEM) in control cells to 55.28 ± 6.75 (SEM) in Vps33B KD cells and to 50.53 ± 6.04 (SEM) in Vps33A KD cells (left panel). Also, the intensity of DQ-BSA fluorescent compartments was reduced ~2.4×, from $117\,626.1 \pm 7804.84$ (SEM) arbitrary units (AU) in control cells to $49\,835.41 \pm 3808$ AU in Vps33B KD cells and ~2× [$63\,575.34 \pm 9563.43$ (SEM)] in Vps33A KD cells (right panels). Error bars represent the standard error of the mean, p-values were analyzed using a 2-tailed t-test with equal variance and related to the scrambled sample. ***$p < 0.001$.

of 4 h to accumulate sufficient fluorescent signal in lysosomes. To monitor fluid phase endocytosis, we added dextran-FITC concomitantly with DQ-BSA.

Depletion of Vps33B clearly reduced DQ-BSA fluorescence (Figure 5A). By quantitation of these data, we found that both the number of compartments displaying DQ fluorescence as well as the average intensity per compartment were decreased in Vps33B KD cells (Figure 5B). Similar results were observed in Vps33A depleted cells (Figure 5) and previously seen after Vps39 or Vps41 KD (58). Notably, using this protocol, we found that dextran-FITC after 4 h uptake accumulates in the perinuclear area of Vps33B KD cells (Figure 5A). This differs from the dispersed pattern seen after 2 h uptake (Figure 1), indicating that Vps33B KD causes a delay rather than a block in the delivery of endocytosed cargo to LE–lysosomal compartments. Together these data suggest that delivery of endocytosed cargo to LEs and lysosomes is delayed in Vps33B KD cells, resulting in a decreased level of degradation.

Vps33B depletion does not impair lysosomal enzyme delivery or catalytic activity

To determine whether the decreased degradative capacity in Vps33B KD cells might be the result of decreased

catalytic enzyme activity, we performed several assays. First, we analyzed the acidity of the LAMP-1-mGFP-positive compartments, since lysosomal enzyme activity requires an acidic pH. Vps33B KD, LAMP-1-mGFP transfected HeLa cells were incubated with Lysotracker™ red, a membrane-permeable molecule that becomes fluorescent in acidic environments (Figure 6A). Both in control and Vps33B KD cells, Lysotracker colocalized with LAMP-1-mGFP, indicating that the accumulated endo-lysosomal compartments in Vps33B KD cells are acidified.

Second, to directly assess lysosomal enzyme activity, we made use of the membrane-permeable substrate magic red cathepsin B (MR Cat B), which reaches endo-lysosomal compartments independent of endocytosis. The MR fluorophore becomes fluorescent only after hydrolysis by the lysosomal cysteine protease cathepsin B at a specific Arg-Arg target sequence. Hence, MR Cat B monitors cathepsin B activity. In control cells, an optimal signal to noise ratio was obtained after 3 h incubation with MR Cat B. Control or Vps33B KD cells were then incubated for 3 h with MR Cat B as well as with dextran-FITC, to visualize the endo-lysosomal system (Figure 6B). Vps33B depletion resulted in a slight (1.2×) increase in dextran-FITC signal and an accumulation in the perinuclear area. These data reinforce the observations shown in Figure 5A and show that the perinuclear accumulation of dextran after prolonged endocytosis is a consistent phenotype upon Vps33B KD. Like dextran, the number of MR cat B fluorescent compartments also slightly (1.3×) increased upon Vps33B KD (Figure 6C). Depletion of Vps33A resulted in a comparable phenotype. The increased number of active cathepsin B-positive compartments after Vps33A or Vps33B silencing is in agreement with the observed increase in late endosomal compartments (Figure 4). Of note, we found that dextran-positive compartments only partially overlapped with MR Cat B compartments (Figure 6B), which is explained by that MR Cat B, in contrast to dextran, reaches endo-lysosomes independently of endocytosis.

Together these data show that the decreased degradation of endocytosed cargo after Vps33A or Vps33B depletion is not due to a defect in acidity or cathepsinB activity in LEs and lysosomes.

Vps33B is involved in delivery of endocytosed cargo to lysosomes

Collectively, our data show that Vps33B KD cells contain more Rab7-, LAMP-1- and Cathepsin B-active-positive compartments, i.e. LE/lysosomal compartments, yet that degradation of endocytosed DQ-BSA is decreased. Importantly, the dextran uptake experiments (i.e. 2 h versus 3 h and 4 h shown in Figures 1, 5 and 6) reveal that Vps33B KD delays delivery of endocytosed cargo to accumulated LAMP-1-positive compartments. Since DQ-BSA follows the constitutive endocytic pathway, like dextran, this predicts that DQ-BSA is also delivered more slowly to lysosomes in Vps33B KD cells, which would explain the observed decrease in degradation. Since both LEs and lysosomes are LAMP-1 positive, the monitoring of cargo delivery to either compartments cannot be discriminated by immunofluorescence, but requires the ultrastructural resolution of EM (58).

To investigate intracellular transport and delivery of endocytosed cargo after Vps33B or Vps33A KD by EM, cells were incubated for 3 h with BSA conjugated to 5 nm gold particles (BSA-Au^5). Cells were fixed and prepared for ultrathin cryosections that were labeled for endogenous LAMP-1 (Figure 7A). Comparison of scrambled versus Vps33B or Vps33A KD cells showed that, in the KD cells, lysosomes were largely devoid of BSA-Au^5. We quantitatively assessed the localization of endocytosed BSA by analyzing endo-lysosomal compartments for their morphology (as described above) and presence of BSA-Au^5 and LAMP-1 (Figure 7B). Our data show that in control cells, endocytosed BSA-Au^5 is readily found in both endosomes and lysosomes, whereas in Vps33B or Vps33A KD cells, lysosomes are significantly devoid of this marker (Figure 7B). The numbers of BSA-Au^5-positive LEs were significantly increased after Vps33B or Vps33A KD, which is in agreement with our quantitation in Figure 4 and add to this that accumulated LEs are reached by endocytic markers.

We conclude that delivery of endocytic cargo to lysosomes is impaired upon KD of either Vps33B or Vps33A. This observation explains the decrease in degradation of DQ-BSA (Figure 5), whereas the increased numbers of BSA-Au^5 containing, LAMP-1 positive LEs corresponds to the increased amount of Dextran (3 h uptake) and

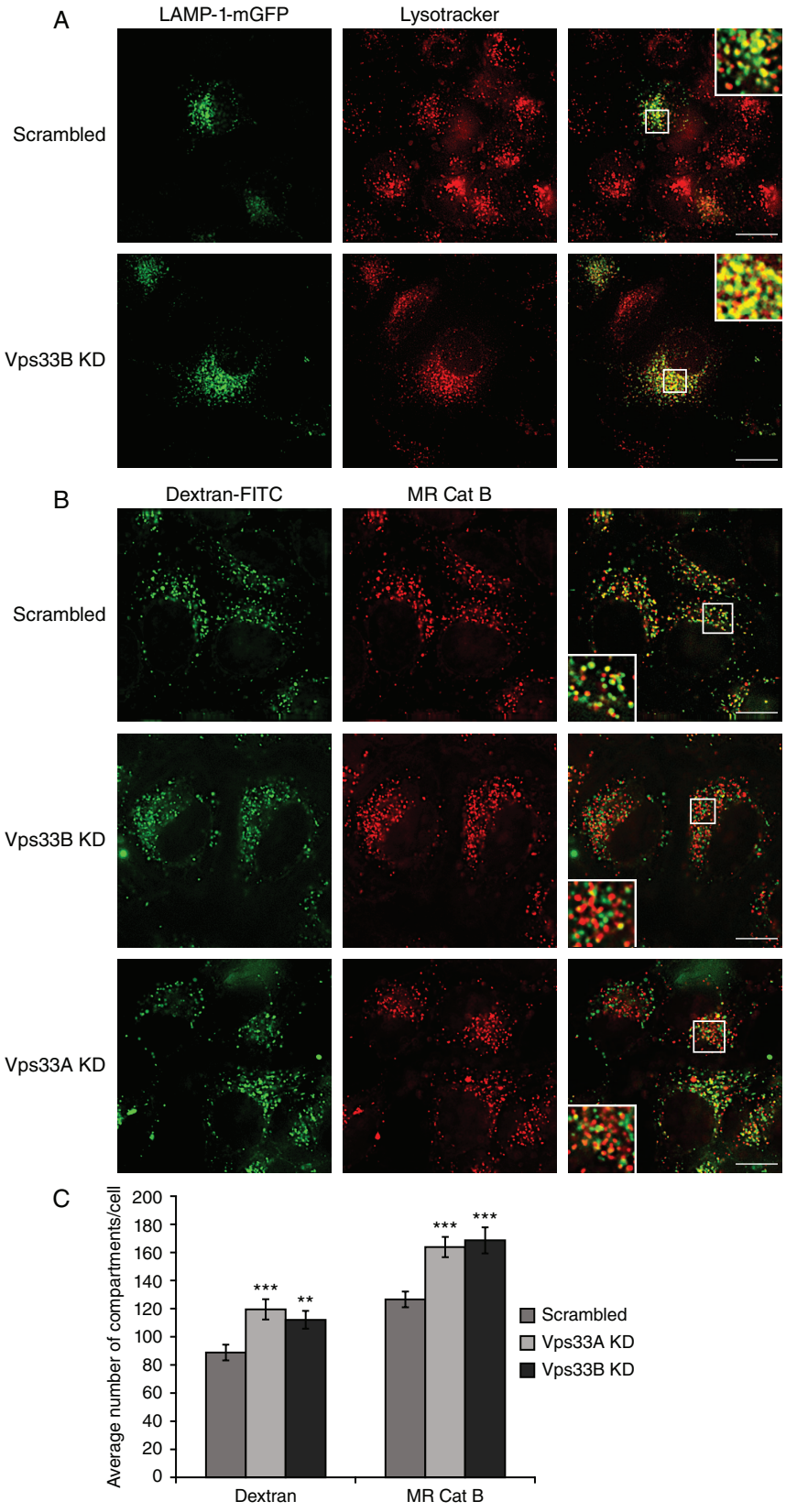

Figure 6: LEs are still acidic and contain activated Cathepsin B after Vps33B depletion. A) Snapshot of live HeLa cells treated with scrambled or Vps33B siRNAs for 3 days, transfected overnight with LAMP-1-mGFP and incubated with Lysotracker™ substrate for 30 min. KD of Vps33B results in the accumulation of LAMP-1-mGFP-positive compartments in the perinuclear region that are positive for Lysotracker™, indicating that the accumulated compartments are acidic. Scale bars, 15 μm. B) Snapshot of live HeLa cells treated with scrambled, Vps33B or Vps33A siRNAs for 3 days and incubated with FITC-conjugated dextran and magic red cathepsin B (MR Cat B) substrate for 3 h. Red fluorescence indicates compartments with active cathepsin B, i.e. able to cleave the membrane-permeable magic red substrate. In all conditions, numerous MR Cat B compartments are present, demonstrating that lysosomal enzymes are activated in the endo-lysosomal system. C) Quantification shows a significant increase of dextran-FITC-positive compartments from 88.8 ± 5.59 (SEM) ($n = 94$ cells) in control cells to 112.1 ± 6.3 (SEM) ($n = 83$ cells) in Vps33B KD cells and to 119.5 ± 7.2 (SEM) ($n = 75$ cells) in Vps33A KD cells as well as MR Cat B compartments from 126.5 ± 5.6 (SEM) compartments in control cells to 168.6 ± 9.3 in Vps33B KD cells and to 163.8 ± 7.3 in Vps33A KD cells. Error bars represent the standard error of the mean. p-Values were analyzed using a 2-tailed t-test with equal variance and related to the scrambled sample. Scale bars, 15 μm. $^{**}p < 0.01$; $^{***}p < 0.001$.

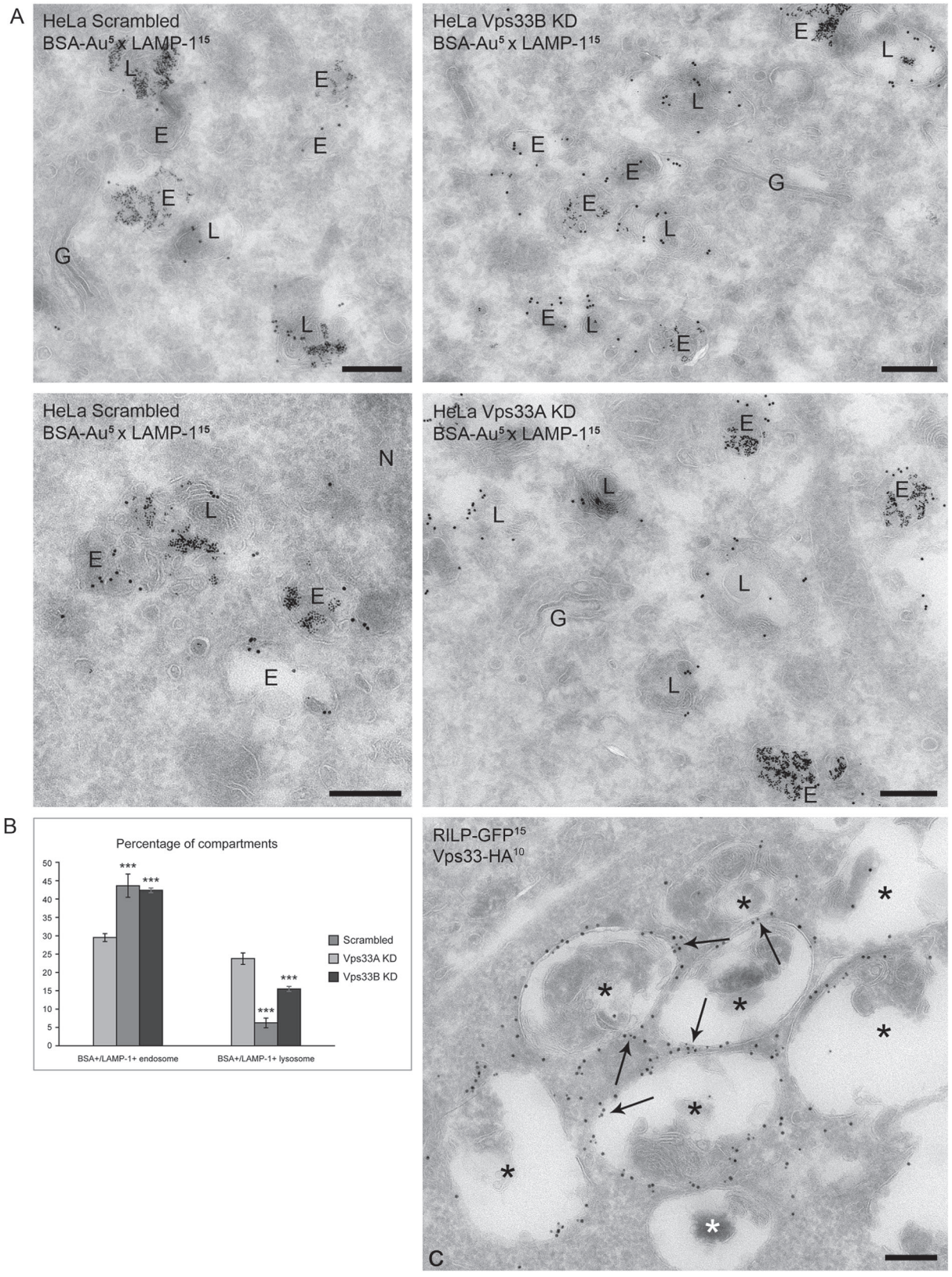

Figure 7: Legend on Next page.

active cathepsinB containing compartments seen by light microscopy (Figure 6). Of note, the effects of Vps33B or Vps33A KD show the same trends, with a slightly stronger effect upon Vps33A KD.

Vps33B localizes to late endosomal and lysosomal compartments when co-expressed with RILP

Our data indicate a role for VPS33B in LE–lysosome fusion and hence efficient delivery of endocytosed cargo to lysosomes. This raised the question of whether Vps33B can associate with endo-lysosomal membranes. In a previous study we showed that exogenously expressed Vps33B is mainly cytosolic, but when over-expressed together with VIPAS-39, it is recruited to recycling endosomes as was determined by immuno-EM (48). These data are in agreement with findings of several groups that Vps33B and VIPAS-39 are not part of CORVET or HOPS (39,45,46,48). Fluorescence studies, however, have shown that Vps33B is recruited to LAMP-1-positive compartments when co-expressed with Rab7-interacting lysosomal protein (RILP) (59). Different from yeast, the mammalian HOPS complex is not recruited to membranes by Rab7 (Ypt7 in yeast), but by binding to Arl8b and RILP that has no apparent ortholog in yeast (59–61). To study the localization of Vps33B in the presence of RILP with ultrastructural resolution, HeLa cells over-expressing Vps33B-HA-V5-His and RILP-GFP were processed for immuno-EM. Over-expression of RILP induces clustering of LEs and lysosomes. We found that Vps33B colocalized with RILP on the cytoplasmic side of the limiting membrane of these clustered LE–lysosomal compartments (Figure 7C). Together these data show that Vps33B is recruited to recycling endosomes when co-expressed with VIPAS-39 and to LEs–lysosomes when co-expressed with RILP.

Vps33A over-expression does not rescue the Vps33B depletion phenotype

Our data show that both Vps33 isoforms are involved in efficient fusion of LEs with lysosomes in mammalian cells. This raised the question whether they can complement each other in the fusion process. To address this, we investigated whether Vps33A over-expression reverses the Vps33B KD phenotype. Scrambled or Vps33B-depleted HeLa cells were co-transfected overnight with LAMP-1-mGFP and Vps33A-HA and analyzed by fluorescence microscopy (Figure 8A). This showed that over-expression of Vps33A-HA does not reverse the peri-nuclear accumulation of LAMP-1-mGFP-positive compartments, the typical phenotype observed after Vps33B depletion.

Our data indicate that Vps33A cannot complement Vps33B function. This finding is in agreement with previous studies showing that *Drosophila* Vps33B does not rescue the loss of Vps33A/Carnation (41) as well as with the fact that Vps33A but not Vps33B is part of the mammalian HOPS complex (38,39,45).

Figure 7: Vps33B KD decreases delivery of endocytic cargo to LAMP-1-positive lysosomes. A) Electron micrographs of ultrathin cryosections of HeLa cells treated with scrambled (left panels), Vps33B siRNAs (upper right panel) or Vps33A (lower right panel) for 3 days. Cells were incubated with BSA-Au^5 for 3 h prior to fixation and subsequently immunogold labeled for endogenous LAMP-1 (15 nm gold particles). Lysosomes present in Vps33B or Vps33A KD cells are consistently more negative for BSA-Au^5 than in control cells. N: nucleus, E: endosome, G: Golgi complex, L: lysosome. Scale bars, 200 nm. B) Quantification of the colocalization of LAMP-1^{15} and BSA-Au^5. Endosomes and lysosomes were distinguished by the presence or absence of BSA-Au^5 and LAMP-1^{15} as well as by morphology. Per condition, two grids in which 200 randomly encountered endo-lysosomes compartments were analyzed. Either Vps33A or Vps33B KD leads to an increase of LEs-containing BSA-Au^5 [from $29.5 \pm 1.08\%$ to $42.375 \pm 0.63\%$ or to $43.625 \pm 3.17\%$ (SD)] in Vps33B or Vps33A KD cells) and a decrease in lysosomes-containing BSA-Au^5 (from $23.75 \pm 1.55\%$ to $15.5 \pm 0.70\%$ or to $6.25 \pm 1.32\%$ (SD) in Vps33B or Vps33A KD cells, respectively), indicating that delivery of endocytosed cargo to lysosomes is impaired. Error bars represent the standard deviation ($n = 4$), p-values were analyzed using a 2-tailed *t*-test with equal variance and related to the scrambled sample. ***$p < 0.001$. C) Electron micrograph of ultrathin cryosection of HeLa cell treated over-expressing Vps33B-HA/V5/his and RILP-GFP labeled for HA (10 nm gold) and GFP (15 nm gold). Vps33B and RILP colocalize at the cytoplasmic site of LE/lysosomal compartments. Scale bars: 200 nm. *: LE/lysosomal. Arrows indicate Vps33B gold labeling on these compartments

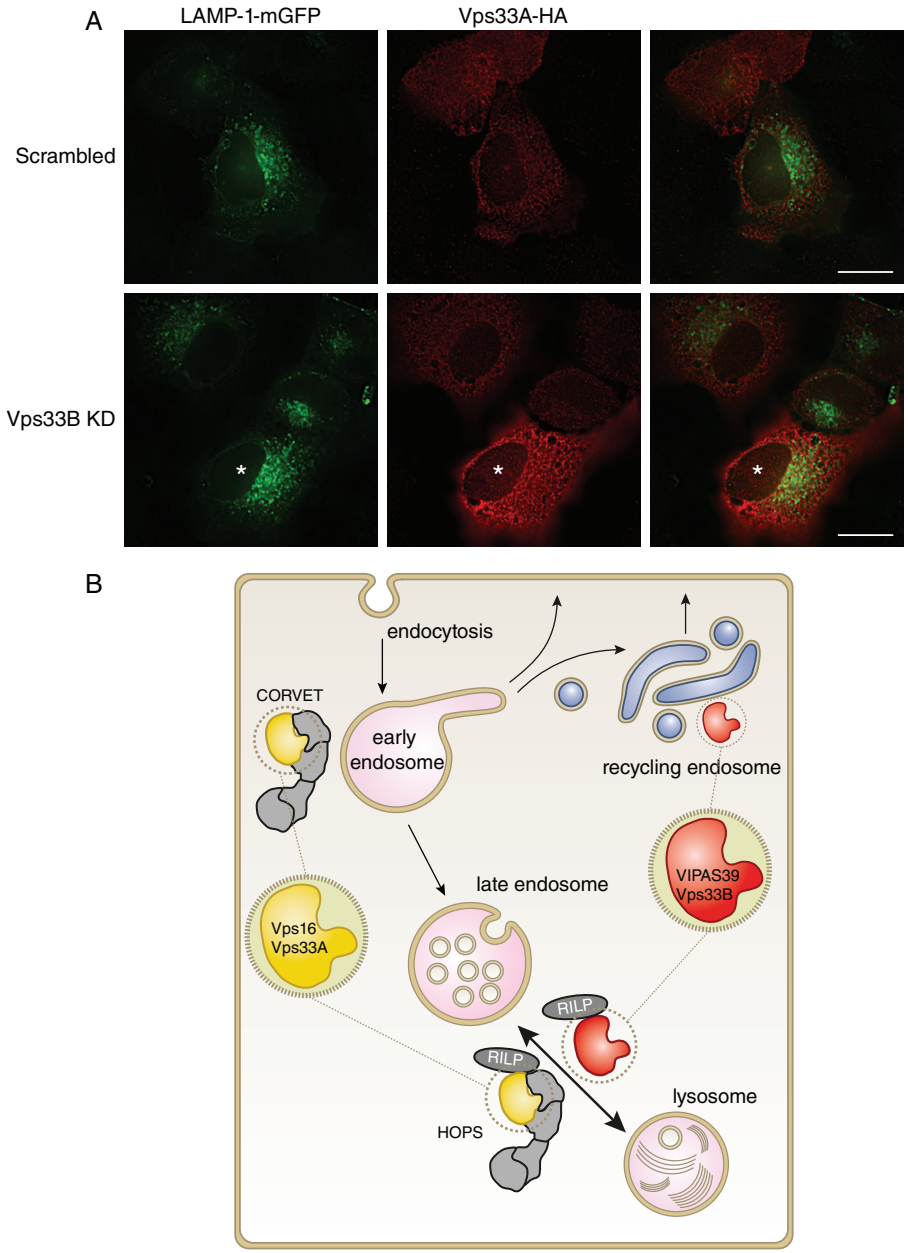

Figure 8: Vps33A does not complement Vps33B function. A) Immunofluorescence of HeLa cells treated with scrambled or Vps33B siRNAs for 3 days and co-transfected overnight with LAMP-1-mGFP and Vps33A-HA. Over-expression of Vps33A (cell indicated by asterisk) does not rescue the accumulation of LAMP-1-mGFP-positive compartments induced after Vps33B depletion. Scale bar, 15 μm. B) Schematic representation of Vps33B function within the endo-lysosomal system of mammalian cells. Vps33B forms a complex with VIPAS-39. When expressed together this complex is recruited to recycling endosomes where it functions in apical recycling in polarized cells. When expressed together with RILP, Vps33B and VIPAS-39 are recruited to LEs–lysosomes, where they are putatively involved in LE–lysosome fusion. Vps33A and Vps16A are also present on LEs and lysosomes where they as part of the HOPS complex are required for LE–lysosome fusion events (38,39,45,58). Hence, both Vps33B/VIPAS-16 and Vps33A/Vps16A-HOPS are required for LE–lysosome fusion, but in distinct complexes. In addition, Vps33A and Vps16A are part of the CORVET complex on early endosomes, which is required for homotypic early endosome fusion (17,30,46). PM: Plasma membrane.

Discussion

Previous studies have implicated a role for Vps33B in endosomal recycling (36,48). In this paper we show that Vps33B is also required for the delivery of endocytosed cargo to lysosomes. A diagram showing the proposed roles of Vps33B, VPS33A and associated proteins in endo-lysosomal fusion events is provided in Figure 8B.

By both light and electron microscopy methods we found that knockdown of Vps33B increased the number of LEs, which is indicative for defective fusion between LEs and lysosomes. Typically, the increased numbers of LEs co-accumulated with lysosomes in the perinuclear region of the cells. By immuno-EM, we showed that significantly more LEs receive endocytosed cargo (BSA-gold), whereas significantly fewer lysosomes were reached by this marker. Concomitantly, degradation of endocytosed DQ-BSA was impaired. We did not find decreased delivery or activation of lysosomal enzymes upon Vps33B or Vps33A KD. Analogous data were obtained after Vps33A depletion. We conclude from our data that endocytic cargos, like DQ-BSA, must reach lysosomes for proper degradation and that this pathway is impaired upon Vps33B or Vps33A KD, most likely through a defect in homotypic LE as well as LE-lysosome fusion events.

In a recent study by Wartosch et al., it was concluded that neither Vps33B nor VIPAS-39 are required for LE fusion with lysosomes (39). This is in apparent contrast to our data showing that Vps33B KD causes an increase in LE numbers and a delay in delivery of endocytic cargo to lysosomes. Notably, however, these authors base their conclusion on the observation that dextran efficiently reaches MR CatB-positive compartments after 2 h pulse/1 h chase. We also find that endocytosed cargo reaches compartments with active cathepsin B after 3 h uptake in Vps33B depleted cells. However, by EM we identify these compartments as LEs, delayed in fusion with lysosomes (Figures 6 and 7). By immunofluorescence LEs and lysosomes cannot easily be distinguished since both are LAMP-1, active Cathepsin B and Rab7 positive.

The notion that Vps33A as well as Vps33B are important for LE-lysosome fusion is reinforced by recent experiments in *C. elegans* showing that both Vps33A and Vps33B are involved in the endosomal maturation process (40). These and our data raise the question whether there are two putative mammalian tethering complexes that function in the LE–lysosomal pathway, containing either Vps33A or Vps33B, as was previously suggested by the Faundez lab (62). An increasing number of studies, including our own non-published findings (v.d. Kant et al., manuscript in submission) show that the mammalian HOPS complex contains Vps16A and Vps33A (38,39,45,46), whereas Vps33B forms a separate complex with VIPAS-39 which acts on recycling endosomes (36,48). Our finding that Vps33A expression does not revert the Vps33B phenotype reinforces the notion that these two close homologues are not part of the same fusion complex. Interestingly, a previous study from the Gissen lab has shown that depletion of VIPAS-39 also induces an increase of LAMP-1-positive LEs/lysosomes (36). Combined these data suggest that the subcomplex formed by Vps33B and VIPAS-39 could function both in the recycling endosome as well as in the endo-lysosomal pathway, but in both locations independently of the HOPS complex. An implication of this finding is that there might be two tethering complexes required for efficient LEs fusion with lysosomes, i.e. HOPS and Vps33B/VIPAS39 (Figure 8B).

The interpretation of our studies, and studies on HOPS/CORVET in general, is hampered by the fact that most endogenous HOPS/CORVET components cannot be detected by microscopy. Hence, we do not know the subcellular localization of endogenous Vps33B in physiological conditions. Exogenous expression of Vps33B results in a cytosolic distribution (36). When co-expressed with VIPAS-39, Vps33B is recruited to Rab11-positive recycling endosomes (36,48), and to LEs-lysosomes when co-expressed with Rab7-interacting lysosomal protein (RILP) (59). RILP is an effector protein of Rab7 that recruits functional dynein-dynactin motor complexes to LEs, which results in their microtubule-dependent transport toward the Golgi region (63). Since RILP recruits components of the HOPS complex as well as Vps33B/VIPAS-39 (59,60), this protein might be a crucial partner for interaction between the HOPS and Vps33B/VIPAS-39 complexes. Interaction of Vps33B/VIPAS-39/ with RILP or Rab11A could control the function of Vps33B in the degradative pathway or on recycling endosomes, respectively. An additional or alternative explanation to explain the role of VPS33B in LE–lysosome fusion would be an indirect

effect through the role of the VPS33B-VIPAS-39 complex on recycling endosomes. However, to the best of our knowledge, impairment of recycling, for example through blocking the formation of recycling tubules (64), does not lead to defects in endo-lysosomal maturation or degradation capacity, which renders this explanation less likely.

The prediction that mammalian homologues of yeast HOPS components function outside the HOPS complex is not new. A similar hypothesis was reached in studies on Vps41. Human Vps41 is part of the HOPS complex, localizes to LEs and lysosomes and is important for lysosome biogenesis (58). However, in addition Vps41 localizes to a subset of TGN-derived carriers that carry LAMP proteins (65). Vps41, but not Vps39 (65) or Vps33B (R. Galmes et al., unpublished observation) is required for fusion of these vesicles with LEs, suggesting a role for Vps41 in and out of the putative mammalian HOPS complex.

Similar to what we show for Vps33B and Vps33A KD cells, depletion of Vps41 or Vps39, the two HOPS complex specific subunits, also lead to an accumulation of LEs and a defect in the delivery of endocytosed cargo to lysosomes (32,58). However, in contrast to Vps39, Vps41 or Vps33A KD, lysosome numbers are not reduced in Vps33B KD cells, as was shown by EM (Figures 3 and 4). Thus, the effect of Vps33B KD on lysosomal biogenesis is milder than that of the other Vps subunits that are studied thus far by the same methodology.

In yeast, Vps33p is part of the HOPS as well as the CORVET complex, which functions in the early endocytic pathway. We found that Rab5 localization was not affected upon Vps33B KD (Figure 2A). This indicates that there is no significant effect of Vps33 KD on EE distribution despite the described role of Vps33B in recycling (36,48). In addition, the Rab5-Rab7 switch was not affected in Vps33B KD cells, as Rab7 was still recruited to endosomes (Figure 2B). Thus, Vps33B KD has no obvious effects on EEs. These data are in agreement with recent studies that describe the mammalian CORVET complex consisting of Vps8, TGFBRAP1 (Vps3 homologue), Vps11, Vps18, Vps16A and Vps33A (46), supporting that Vps33B takes no part in the mammalian CORVET complex located on EEs

In summary, our studies suggest that in addition to its role in the Rab11 endosomal recycling pathways (48), Vps33B could function with VIPAS-39 in LE-lysosomal fusion events

Materials and Methods

Antibodies, reagents and constructs

The LAMP-1 antibody used in this study was monoclonal mouse anti-human LAMP-1 CD107a from BD Pharmingen. Mouse anti-HA (16B12) was purchased from Covance Research Products. Biotinylated goat anti-GFP and rabbit anti-biotin were both purchased from Rockland. Monoclonal mouse anti-actin clone 4 was purchased from ICN biomedicals. Rabbit anti mouse IgG Z0412 was purchased from Dako. Protein A-gold 10, 15 nm and bovine serum albumin gold coupled to 5 nm gold particles (BSA-Au^5) were homemade (Cell Microscopy Center, UMC Utrecht, The Netherlands). MagicRedcathepsin B kit was from Immunochemistry Technologies.

The 10 000 MW dextran-alexa488 or -alexa568 or -FITC, DQ-BSA, Lysotracker™ red, conjugated fluorescent secondary antibodies, cell culture Dulbecco's Modified Eagle Medium, Trypsine, L-glutamine and penicillin/streptomycin were purchased from Life Technologies. Fetal bovine serum (FBS) was purchased from Sigma. Effectene and Hiperfect transfection reagents were purchased from Qiagen. SiRNAs (described below) were purchased from Dharmacon/Thermo Scientific. Human LAMP-1-mGFP was a kind gift from E. Dell'Angelica (UCLA, Los Angeles, California, USA) and described in (66), human Vps33B-HA/V5/his was a kind gift from V. Faundez (Emory University, Atlanta, GA, USA). Human Rab7-eGFP and RILP-GFP were kindly provided by J. Neefjes (Netherlands Cancer Institute (NKI), Amsterdam, The Netherlands). Rab5-eGFP was previously described in (67).

Cell culture, siRNA and transfection

HeLa (ATCC, clone ccl-2) cells were grown at 37°C in DMEM supplemented with 10% heat-inactivated (56°C, 30 min) FBS, 2 mM L-Glutamine, 100 units/mL penicillin and 100μg/mL streptomycin under a 5% CO_2/air atmosphere. KDs were achieved with Allstars negative siRNAs for controls and on-target siGENOME smartpool human Vps33B siRNAs (#1: ggagaggcauggacauuaa, #2: caagauggcauaugaauug, #3: aaacagcgcucgccuuaug, #18: acguguggacggcgaguau) and on-target siGENOME smartpool human Vps33A siRNAs (#1: gaagaaacgucaaccggga, #2: ggcaauaguuugggaugaa, #3: ggcuagaguugauggauau, #4: gggcguaaccuucgcugaa) for 3 days using Hiperfect reagent. HeLa cells were transfected with cDNAs encoding LAMP-1-mGFP overnight orRab5-eGFP or Rab7-eGFP for 8 h using Effectene reagent according to manufacturer's instructions. Efficiency of KD was determined using Q-PCR and samples were only analyzed if results indicate at least a 75% mRNA decrease.

Indirect immunofluorescence and live cell imaging

HeLa cells grown on coverslips for 3 days were washed with PBS, fixed with 4% paraformaldehyde (PFA) for 20 min and subsequently

permeabilized with PBS/0.1% Triton X-100 for 10 min. After blocking in PBS/1% BSA, cells were incubated for 1 h at room temperature with primary antibodies, then for 30 min with fluorescently-labeled secondary antibodies. Coverslips were then mounted on microscopy slides using Prolong Goldantifade reagent (Life Technologies). Images were acquired on a Deltavision wide field microscope. Optical sections were recorded with a 100×/1.4A immersion objective. Fluorescent pictures were collected with an EMCCD camera, deconvolved and analyzed using the SOFTWORX software (Applied Precision). Images were processed using PHOTOSHOP CS5.1 software. Figure compilation was accomplished using PHOTOSHOP CS5.1. For the live cell imaging experiments HeLa cells were grown on coverslips and incubated with fluorescently-conjugated probes (i.e. dextrans, DQ-BSA and MR cathepsin B). Then the coverslips were washed 3 times with PBS and transferred to warmed MEM Hanks without phenol red supplemented with 2.5% FBS. Cells were kept at 37°C/5% CO_2 using a climate chamber. Snapshots were acquired as described above. Quantifications were done using VOLOCITY software (PerkinElmer) on at least three distinct experiments. Profile line quantifications were done using IMAGEJ software.

Quantitative immuno-electron microscopy

HeLa cells were grown in 60 mm-dish and transfected as described above. HeLa cells were fixed by adding freshly prepared 4% PFA (paraformaldehyde) (wt/vol) (Polysciences) in 0.1 M phosphate buffer (pH 7.4) to an equal volume of culture medium for 10 min, followed by post-fixation in 4% PFA (wt/vol) at 4°C overnight. Ultrathin cryosectioning and immunogold labeling were performed as described in (68): Fixed cells were incubated with PBS containing 0.05 M glycine, gently scraped free, and embedded in 12% gelatin in PBS. The cell pellet was solidified on ice and cut into small blocks. For cryoprotection, blocks were infiltrated overnight with 2.3 M sucrose at 4°C and then mounted on pins and frozen in liquid nitrogen. Ultrathin cryosections (70 nm) were prepared on a Leica ultracut UCT ultra cryo-microtome and picked up with a freshly prepared 1:1 mixture of 2.3 M sucrose and 1.8% methylcellulose (69). Sections were then immunogold-labeled and examined using a JEOL TEM 1010 electron microscope at 80 kV.

Epon flat embedding

HeLa cells were grown and treated with scrambled or Vps33B siRNAs in 60 mm-dish for 3 days and fixed with a mixture of 2% glutaraldehyde, 5 mM $CaCl_2$, 10 mM $MgCl_2$ in 0.1 M Na-cacodylate buffer pH 7.4 for 4 h at room temperature. Postfixation was performed in 1% OsO_4, 1.5% $K_4Fe(Cn)_6$-$3H_2O$ in distilled water for 2 h at 4°C. After ethanol dehydration, cells were flat embedded in Epon and sectioned in parallel to the substrate of growth. Ultrathin sections were stained with uranylacetate and lead citrate. Sections were examined using a JEOL TEM 1010 electron microscope at 60 kV.

Western blot

For western blot, HeLa cells grown in 6 cm dish were lysed in 250 µL 1% Triton-X-100, dithiothreitol (DTT) and phenylmethanesulfonylfluoride (PMSF) for 20 min on ice. Lysates were cleared by centrifugation and collected in 5× Laemmli buffer containing 10% SDS, 50% glycerol, 0.625 M Tris pH 6.8, 250 mM DTT and 0.01% Bromophenol blue. Samples were separated on 12% SDS-PAGE gels and blotted on Immobilon-FL PVDF (Millipore). Blots were analyzed for HA and actin using primary antibodies described above. Secondary alexa680 or IrDye800 fluorescent antibodies were used for detection in the Odyssey imaging system (Li-Cor). Antibody incubations were typically 1 h, followed by five washing step in blocking buffer (Li-Cor).

Acknowledgments

We want to thank M. Spit, C. Rabouille, and A. Grieve for critically reading this manuscript. We thank Cilia de Heus for help with sample preparation and express our special thanks to Rene Scriwanek for preparation of the electron micrographs and editing the figures. We thank Esteban Dell'Angelica, Victor Faundez and Jacques Neefjes for providing constructs. R. G. is supported by VICI grant 918.56.611 of the Netherlands Organization for Scientific Research (NWO) that was awarded to J. K.

References

1. Rink J, Ghigo E, Kalaidzidis Y, Zerial M. Rab conversion as a mechanism of progression from early to late endosomes. Cell 2005;122:735–749.
2. Mullock BM, Bright NA, Fearon CW, Gray SR, Luzio JP. Fusion of lysosomes with late endosomes produces a hybrid organelle of intermediate density and is NSF dependent. J Cell Biol 1998;140:591–601.
3. Luzio JP, Pryor PR, Bright NA. Lysosomes: fusion and function. Nat Rev Mol Cell Biol 2007;8:622–632.
4. Huotari J, Helenius A. Endosome maturation. EMBO J 2011;30:3481–3500.
5. Mellman I, Fuchs R, Helenius A. Acidification of the endocytic and exocytic pathways. Annu Rev Biochem 1986;55:663–700.
6. van Meel E, Klumperman J. Imaging and imagination: understanding the endo-lysosomal system. Histochem Cell Biol 2008;129:253–266.
7. Ohya T, Miaczynska M, Coskun U, Lommer B, Runge A, Drechsel D, Kalaidzidis Y, Zerial M. Reconstitution of Rab- and SNARE-dependent membrane fusion by synthetic endosomes. Nature 2009;459:1091–1097.
8. Cai H, Reinisch K, Ferro-Novick S. Coats, tethers, Rabs, and SNAREs work together to mediate the intracellular destination of a transport vesicle. Dev Cell 2007;12:671–682.
9. Whyte JR, Munro S. Vesicle tethering complexes in membrane traffic. J Cell Sci 2002;115:2627–2637.
10. McNew JA, Parlati F, Fukuda R, Johnston RJ, Paz K, Paumet F, Sollner TH, Rothman JE. Compartmental specificity of cellular membrane fusion encoded in SNARE proteins. Nature 2000;407:153–159.
11. Jahn R, Scheller RH. SNAREs--engines for membrane fusion. Nat Rev Mol Cell Biol 2006;7:631–643.
12. Carr CM, Rizo J. At the junction of SNARE and SM protein function. Curr Opin Cell Biol 2010;22:488–495.

13. Seals DF, Eitzen G, Margolis N, Wickner WT, Price A. A Ypt/Rab effector complex containing the Sec1 homolog Vps33p is required for homotypic vacuole fusion. Proc Natl Acad Sci U S A 2000;97:9402–9407.
14. Sacher M, Jiang Y, Barrowman J, Scarpa A, Burston J, Zhang L, Schieltz D, Yates JR 3rd, Abeliovich H, Ferro-Novick S. TRAPP, a highly conserved novel complex on the cis-Golgi that mediates vesicle docking and fusion. EMBO J 1998;17:2494–2503.
15. Ungar D, Oka T, Brittle EE, Vasile E, Lupashin VV, Chatterton JE, Heuser JE, Krieger M, Waters MG. Characterization of a mammalian Golgi-localized protein complex, COG, that is required for normal Golgi morphology and function. J Cell Biol 2002;157:405–415.
16. TerBush DR, Maurice T, Roth D, Novick P. The Exocyst is a multiprotein complex required for exocytosis in Saccharomyces cerevisiae. EMBO J 1996;15:6483–6494.
17. Peplowska K, Markgraf DF, Ostrowicz CW, Bange G, Ungermann C. The CORVET tethering complex interacts with the yeast Rab5 homolog Vps21 and is involved in endo-lysosomal biogenesis. Dev Cell 2007;12:739–750.
18. Nickerson DP, Brett CL, Merz AJ. Vps-C complexes: gatekeepers of endolysosomal traffic. Curr Opin Cell Biol 2009;21:543–551.
19. Rieder SE, Emr SD. A novel RING finger protein complex essential for a late step in protein transport to the yeast vacuole. Mol Biol Cell 1997;8:2307–2327.
20. Wurmser AE, Sato TK, Emr SD. New component of the vacuolar class C-Vps complex couples nucleotide exchange on the Ypt7 GTPase to SNARE-dependent docking and fusion. J Cell Biol 2000;151:551–562.
21. Brocker C, Kuhlee A, Gatsogiannis C, Balderhaar HJ, Honscher C, Engelbrecht-Vandre S, Ungermann C, Raunser S. Molecular architecture of the multisubunit homotypic fusion and vacuole protein sorting (HOPS) tethering complex. Proc Natl Acad Sci U S A 2012;109:1991–1996.
22. Ostrowicz CW, Brocker C, Ahnert F, Nordmann M, Lachmann J, Peplowska K, Perz A, Auffarth K, Engelbrecht-Vandre S, Ungermann C. Defined subunit arrangement and rab interactions are required for functionality of the HOPS tethering complex. Traffic 2010;11:1334–1346.
23. Cabrera M, Ostrowicz CW, Mari M, LaGrassa TJ, Reggiori F, Ungermann C. Vps41 phosphorylation and the Rab Ypt7 control the targeting of the HOPS complex to endosome-vacuole fusion sites. Mol Biol Cell 2009;20:1937–1948.
24. Plemel RL, Lobingier BT, Brett CL, Angers CG, Nickerson DP, Paulsel A, Sprague D, Merz AJ. Subunit organization and Rab interactions of Vps-C protein complexes that control endolysosomal membrane traffic. Mol Biol Cell 2011;22:1353–1363.
25. Stroupe C, Collins KM, Fratti RA, Wickner W. Purification of active HOPS complex reveals its affinities for phosphoinositides and the SNARE Vam7p. EMBO J 2006;25:1579–1589.
26. Kramer L, Ungermann C. HOPS drives vacuole fusion by binding the vacuolar SNARE complex and the Vam7 PX domain via two distinct sites. Mol Biol Cell 2011;22:2601–2611.
27. Subramanian S, Woolford CA, Jones EW. The Sec1/Munc18 protein, Vps33p, functions at the endosome and the vacuole of Saccharomyces cerevisiae. Mol Biol Cell 2004;15:2593–2605.
28. Lobingier BT, Merz AJ. Sec1/Munc18 protein Vps33 binds to SNARE domains and the quaternary SNARE complex. Mol Biol Cell 2012;23:4611–4622.
29. Peplowska K, Markgraf DF, Ostrowicz CW, Bange G, Ungermann C. The CORVET tethering complex interacts with the yeast Rab5 homolog Vps21 and is involved in endo-lysosomal biogenesis. Dev Cell 2007;12:739–750.
30. Balderhaar HJ, Lachmann J, Yavavli E, Brocker C, Lurick A, Ungermann C. The CORVET complex promotes tethering and fusion of Rab5/Vps21-positive membranes. Proc Natl Acad Sci U S A 2013;110:3823–3828.
31. Kim BY, Kramer H, Yamamoto A, Kominami E, Kohsaka S, Akazawa C. Molecular characterization of mammalian homologues of class C Vps proteins that interact with syntaxin-7. J Biol Chem 2001;276:29393–29402.
32. Caplan S, Hartnell LM, Aguilar RC, Naslavsky N, Bonifacino JS. Human Vam6p promotes lysosome clustering and fusion in vivo. J Cell Biol 2001;154:109–122.
33. McVey Ward D, Radisky D, Scullion MA, Tuttle MS, Vaughn M, Kaplan J. hVPS41 is expressed in multiple isoforms and can associate with vesicles through a RING-H2 finger motif. Exp Cell Res 2001;267:126–134.
34. Huizing M, Didier A, Walenta J, Anikster Y, Gahl WA, Kramer H. Molecular cloning and characterization of human VPS18, VPS 11, VPS16, and VPS33. Gene 2001;264:241–247.
35. Pulipparacharuvil S, Akbar MA, Ray S, Sevrioukov EA, Haberman AS, Rohrer J, Kramer H. Drosophila Vps16A is required for trafficking to lysosomes and biogenesis of pigment granules. J Cell Sci 2005;118:3663–3673.
36. Cullinane AR, Straatman-Iwanowska A, Zaucker A, Wakabayashi Y, Bruce CK, Luo G, Rahman F, Gurakan F, Utine E, Ozkan TB, Denecke J, Vukovic J, Di Rocco M, Mandel H, Cangul H, et al. Mutations in VIPAR cause an arthrogryposis, renal dysfunction and cholestasis syndrome phenotype with defects in epithelial polarization. Nat Genet 2010;42:303–312.
37. Zhu GD, Salazar G, Zlatic SA, Fiza B, Doucette MM, Heilman CJ, Levey AI, Faundez V, L'Hernault SW. SPE-39 family proteins interact with the HOPS complex and function in lysosomal delivery. Mol Biol Cell 2009;20:1223–1240.
38. Graham SC, Wartosch L, Gray SR, Scourfield EJ, Deane JE, Luzio JP, Owen DJ. Structural basis of Vps33A recruitment to the human HOPS complex by Vps16. Proc Natl Acad Sci U S A 2013;110:13345–13350.
39. Wartosch L, Gunesdogan U, Graham SC, Luzio JP. Recruitment of VPS33A to HOPS by VPS16 Is required for lysosome fusion with endosomes and autophagosomes. Traffic 2015;16:727–742.
40. Solinger JA, Spang A. Loss of the Sec1/Munc18-family proteins VPS-33.2 and VPS-33.1 bypasses a block in endosome maturation in *Caenorhabditis elegans*. Mol Biol Cell 2014;25:3909–3925.

41. Akbar MA, Ray S, Kramer H. The SM protein Car/Vps33A regulates SNARE-mediated trafficking to lysosomes and lysosome-related organelles. Mol Biol Cell 2009;20:1705–1714.
42. Sriram V, Krishnan KS, Mayor S. Deep-orange and carnation define distinct stages in late endosomal biogenesis in Drosophila melanogaster. J Cell Biol 2003;161:593–607.
43. Guo X, Tu L, Gumper I, Plesken H, Novak EK, Chintala S, Swank RT, Pastores G, Torres P, Izumi T, Sun TT, Sabatini DD, Kreibich G. Involvement of vps33a in the fusion of uroplakin-degrading multivesicular bodies with lysosomes. Traffic 2009;10:1350–1361.
44. Suzuki T, Oiso N, Gautam R, Novak EK, Panthier JJ, Suprabha PG, Vida T, Swank RT, Spritz RA. The mouse organellar biogenesis mutant buff results from a mutation in Vps33a, a homologue of yeast vps33 and Drosophila carnation. Proc Natl Acad Sci U S A 2003;100:1146–1150.
45. Jiang P, Nishimura T, Sakamaki Y, Itakura E, Hatta T, Natsume T, Mizushima N. The HOPS complex mediates autophagosome-lysosome fusion through interaction with syntaxin 17. Mol Biol Cell 2014;25:1327–1337.
46. Perini ED, Schaefer R, Stoter M, Kalaidzidis Y, Zerial M. Mammalian CORVET is required for fusion and conversion of distinct early endosome subpopulations. Traffic 2014;15:1366–1389.
47. Gissen P, Johnson CA, Morgan NV, Stapelbroek JM, Forshew T, Cooper WN, McKiernan PJ, Klomp LW, Morris AA, Wraith JE, McClean P, Lynch SA, Thompson RJ, Lo B, Quarrell OW, et al. Mutations in VPS33B, encoding a regulator of SNARE-dependent membrane fusion, cause arthrogryposis-renal dysfunction-cholestasis (ARC) syndrome. Nat Genet 2004;36:400–404.
48. Smith H, Galmes R, Gogolina E, Straatman-Iwanowska A, Reay K, Banushi B, Bruce CK, Cullinane AR, Romero R, Chang R, Ackermann O, Baumann C, Cangul H, Celik FC, Aygun C, et al. Associations among genotype, clinical phenotype and intracellular localization of trafficking proteins in ARC syndrome. Hum Mutat 2012;33: 1656–1664.
49. Lock JG, Stow JL. Rab11 in recycling endosomes regulates the sorting and basolateral transport of E-cadherin. Mol Biol Cell 2005;16:1744–1755.
50. van Ijzendoorn SC. Recycling endosomes. J Cell Sci 2006;119:1679–1681.
51. van ISC, Hoekstra D. The subapical compartment: a novel sorting centre? Trends Cell Biol 1999;9:144–149.
52. Urban D, Li L, Christensen H, Pluthero FG, Chen SZ, Puhacz M, Garg PM, Lanka KK, Cummings JJ, Kramer H, Wasmuth JD, Parkinson J, Kahr WH. The VPS33B-binding protein VPS16B is required in megakaryocyte and platelet alpha-granule biogenesis. Blood 2012;120:5032–5040.
53. Lo B, Li L, Gissen P, Christensen H, McKiernan PJ, Ye C, Abdelhaleem M, Hayes JA, Williams MD, Chitayat D, Kahr WH. Requirement of VPS33B, a member of the Sec1/Munc18 protein family, in megakaryocyte and platelet alpha-granule biogenesis. Blood 2005;106:4159–4166.
54. Akbar MA, Tracy C, Kahr WHA, Kramer H. The full-of-bacteria gene is required for phagosome maturation during immune defense in Drosophila. J Cell Biol 2011;192:383–390.
55. Bach H, Papavinasasundaram KG, Wong D, Hmama Z, Av-Gay Y. Mycobacterium tuberculosis virulence is mediated by PtpA dephosphorylation of human vacuolar protein sorting 33B. Cell Host Microbe 2008;3:316–322.
56. Poteryaev D, Datta S, Ackema K, Zerial M, Spang A. Identification of the switch in early-to-late endosome transition. Cell 2010;141:497–508.
57. Kobayashi T, Startchev K, Whitney AJ, Gruenber J. Localization of lysobisphosphatidic acid-rich membrane domains in late endosomes. Biol Chem 2001;382:483–485.
58. Pols MS, ten Brink C, Gosavi P, Oorschot V, Klumperman J. The HOPS proteins hVps41 and hVps39 are required for homotypic and heterotypic late endosome fusion. Traffic 2013;14:219–232.
59. van der Kant R, Fish A, Janssen L, Janssen H, Krom S, Ho N, Brummelkamp T, Carette J, Rocha N, Neefjes J. Late endosomal transport and tethering are coupled processes controlled by RILP and the cholesterol sensor ORP1L. J Cell Sci 2013;126:3462–3474.
60. Lin X, Yang T, Wang S, Wang Z, Yun Y, Sun L, Zhou Y, Xu X, Akazawa C, Hong W, Wang T. RILP interacts with HOPS complex via VPS41 subunit to regulate endocytic trafficking. Sci Rep 2014;4:7282.
61. Garg S, Sharma M, Ung C, Tuli A, Barral DC, Hava DL, Veerapen N, Besra GS, Hacohen N, Brenner MB. Lysosomal trafficking, antigen presentation, and microbial killing are controlled by the Arf-like GTPase Arl8b. Immunity 2011;35:182–193.
62. Zlatic SA, Tornieri K, L'Hernault SW, Faundez V. Metazoan cell biology of the HOPS tethering complex. Cell Logist 2011;1:111–117.
63. Jordens I, Fernandez-Borja M, Marsman M, Dusseljee S, Janssen L, Calafat J, Janssen H, Wubbolts R, Neefjes J. The Rab7 effector protein RILP controls lysosomal transport by inducing the recruitment of dynein-dynactin motors. Curr Biol 2001;11:1680–1685.
64. Delevoye C, Miserey-Lenkei S, Montagnac G, Gilles-Marsens F, Paul-Gilloteaux P, Giordano F, Waharte F, Marks MS, Goud B, Raposo G. Recycling endosome tubule morphogenesis from sorting endosomes requires the kinesin motor KIF13A. Cell Rep 2014;6:445–454.
65. Pols MS, van Meel E, Oorschot V, ten Brink C, Fukuda M, Swetha MG, Mayor S, Klumperman J. hVps41 and VAMP7 function in direct TGN to late endosome transport of lysosomal membrane proteins. Nat Commun 2013;4:1361.
66. Falcon-Perez JM, Nazarian R, Sabatti C, Dell'Angelica EC. Distribution and dynamics of Lamp1-containing endocytic organelles in fibroblasts deficient in BLOC-3. J Cell Sci 2005;118:5243–5255.
67. Deneka M, Neeft M, Popa I, van Oort M, Sprong H, Oorschot V, Klumperman J, Schu P, van der Sluijs P. Rabaptin-5alpha/rabaptin-4 serves as a linker between rab4 and gamma(1)-adaptin in membrane recycling from endosomes. EMBO J 2003;22:2645–2657.
68. Slot JW, Geuze HJ. Cryosectioning and immunolabeling. Nat Protoc 2007;2:2480–2491.
69. Liou W, Geuze HJ, Slot JW. Improving structural integrity of cryosections for immunogold labeling. Histochem Cell Biol 1996;106:41–58.